ACS OMEGA

http://pubs.acs.org/journal/acsodf

Article

Experimental Study on the Effect of Pitch Sloshing on the Heat Transfer and Pressure Drop of an LNG Spiral-Wound Heat Exchanger

Longfei Dong,* Hao Wang, Xiao Wu, Yanping Xin, Shunyao Jiang, Hailei Yao, and Yanling Huo

Cite This: *ACS Omega* 2023, 8, 27467−27481

Read Online

ACCESS | Metrics & More | Article Recommendations

ABSTRACT: With the development and utilization of offshore liquefied natural gas, it is increasingly important to study the influence of the heat transfer performance of a spiral-wound heat exchanger under sloshing conditions. This study focused on the effects of different sloshing amplitudes and sloshing periods on the heat transfer and pressure drop performance of a heat exchanger. Through experimental research, the results showed that the fluctuation of the UA (U is the heat transfer coefficient; A is the heat exchange area) value first increased and then decreased with an increase in the sloshing amplitude. The UA value increased by 12.92% and decreased by 42.03% compared to the static value at 3 and 9°, respectively. The fluctuation in the UA value first decreased and then increased with an increase in the sloshing period. The UA value decreased by 36.66% and increased by 10.82% slowly compared to the static value when the sloshing period was 6 and 20 s, respectively. Based on this, a mathematical model of heat transfer under the condition of pitch sloshing was established.

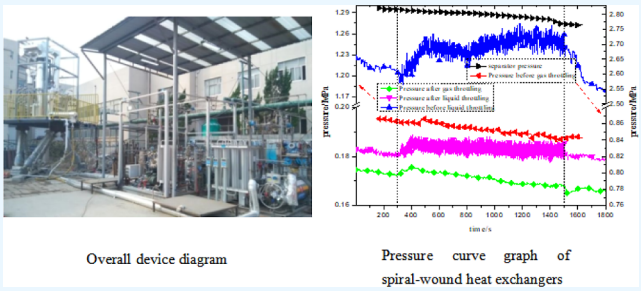

Overall device diagram

Pressure curve graph of spiral-wound heat exchangers

1. INTRODUCTION

Spiral-wound heat exchangers (Figure 1) are primarily used in large onshore natural gas liquefaction plants and large liquefied natural gas (LNG) floating production storage and offloading unit processes for natural gas liquefaction. Its structure is shown in Figure 1. The different tubes are coiled in layers around the central core. The coiling direction alternates from one layer to the next. Radial and longitudinal distances between the tubes are held constant by use of space bars. The tubes are connected to tube sheets at both ends of the heat exchanger.[1] As the main equipment in the liquefaction process, the heat transfer and flow performance of the spiral-wound heat exchanger directly affect the selection of other equipment and the scale of the liquefaction process. Therefore, research on their heat transfer and flow characteristics has gradually increased in recent years.

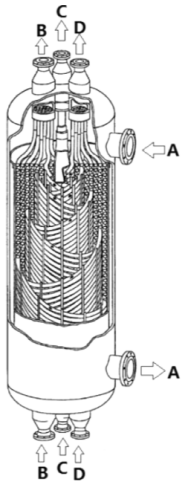

Figure 1. Schematic of the geometric structure of the LNG coil heat exchanger.

Neeraas et al.[1,2] developed a calculation method for the heat transfer and pressure drop when the gas flowed around the shell side of the heat exchanger. Li et al.[3,4] established a numerical model of two-phase boiling heat transfer through numerical simulations and an experimental comparison. Based on this, the effects of radial tube spacing and tube diameter on the shell-side flow pattern and heat transfer characteristics were investigated. Genic et al.[5] summarized a shell-side heat transfer correlation suitable for Re = 1000−9000 through an experimental analysis of three heat exchangers. Abolmaali et al.[6] determined the heat transfer coefficient in the heat leakage calculation by studying the heat transfer mechanism between the shell-side fluid and shell wall of a spiral-wound heat

Received: April 30, 2023
Accepted: July 12, 2023
Published: July 21, 2023

exchanger. Jian et al.[7] experimentally studied the shell-side condensation mechanism of a tubular heat exchanger and found that the heat transfer of the lower pipe was the main heat transfer mode in the entire test section, and increasing the pipe spacing led to a decrease in the shell-side condensation heat transfer coefficient. Zheng et al.[8] designed a disc distributor and experimentally analyzed the working fluid distribution under sloshing conditions and found that the influence of the vertical sloshing condition on the fluid was the smallest. Through experiments, Sharqawy et al.[9] studied the influence of the flow structure on the performance of a heat exchanger, and Hu et al.[10] established a heat transfer coefficient formula for mixed hydrocarbon refrigerant shell-side boiling. Tang et al.[11] found that the pressure drop and heat transfer coefficient of a gas-phase fluid on the shell side decreased with an increase in the winding angle. By establishing a three-dimensional numerical model, Zeng et al.[12] found that geometric parameters, such as the outer diameter of the heat exchange tube, number of layers of the heat exchange tube, and axial spacing of the first layer of the heat exchange tube, have an important influence on the heat transfer performance and flow performance. Lu et al.[13] found that the selection of a constant wall temperature boundary condition was more accurate than that of a constant heat flux boundary condition through the numerical simulation of a three-layer spiral-wound heat exchanger.

Research interest in the heat transfer performance of tube-wound heat exchangers under rolling conditions has grown annually. Li et al.[14] simulated the change in the heat transfer performance of a transverse tube and an elliptical cross-sectional sine wave tube under rolling conditions. Ren[15−17] simulated the heat transfer and pressure drop characteristics of superheated alkane gas and two-phase alkane gas on the shell side of a tube heat exchanger under pitch and heave conditions. Sun et al.[18,19] compared and studied the changes in the thermal parameters of the tube side and shell side under different sloshing conditions. Wang et al.[20] simulated the effect of different sloshing amplitudes and periods on heat transfer performance under pitch conditions. Zheng et al.[21] found that under steady-state, heave, and pitch conditions, the uniformity of the fluid distribution improved with an increase in the mass flow rate. Duan et al.[22] established a three-dimensional dynamic model and found that the uneven distribution of the shell side caused by sloshing led to a fluctuation in the heat transfer performance within 8%. Fouling may be formed on the outer surface of the heat exchange tube during the heat transfer process of the shell-side refrigerant falling film. Mu et al.[26,27] investigated the physical−chemical properties of divalent copper and divalent calcium alginate bulk films and their anti-biofouling activity toward, for example, Chlorella vulgaris and in a natural river water environment.

Currently, research on tubular heat exchangers mainly focuses on land-based conditions, whereas the change in heat transfer and flow performance under sea sloshing conditions is mainly studied by numerical simulation. Therefore, here, a method of experimental research is adopted to study the effect of different sloshing amplitudes and sloshing periods on the heat transfer and pressure drop performance of the heat exchanger under the condition of longitudinal sloshing; the experimental analysis reveals the law of heat transfer and pressure drop under the pitching condition.

2. EXPERIMENTAL DEVICE AND MEASUREMENT DEVIATION

2.1. Experimental Device. The experiment adopted the dual mixed refrigerant refrigeration process, as shown in Figure 2;[25] the experimental device was divided into three modules:

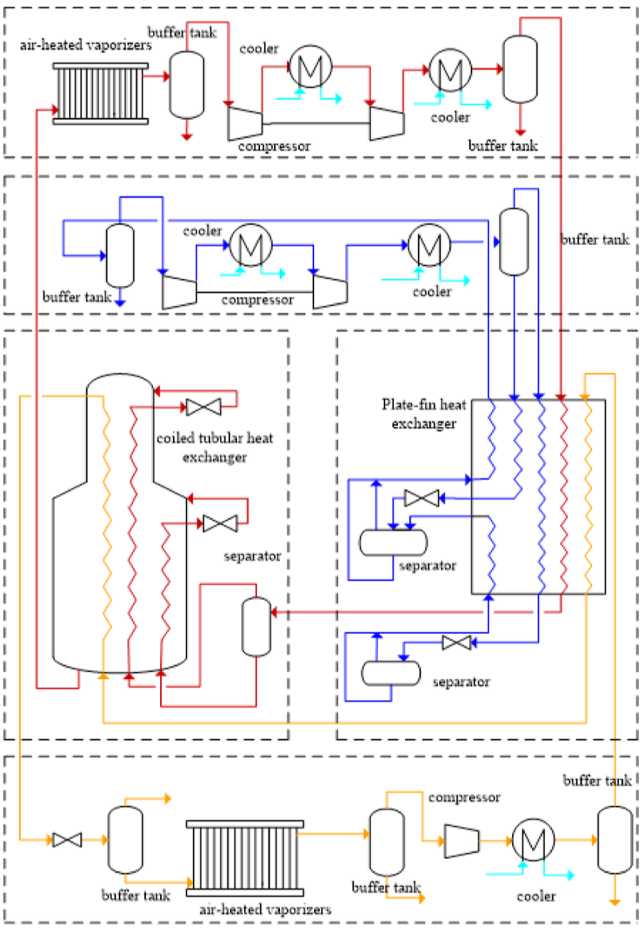

Figure 2. Flow diagram of the double-mixing refrigerant (reproduced from Dong L F, Wu X, Liu K, Sun Q C. Influence of Sloshing Conditions on the Pressure Drop and Heat Transfer of a Single-Layer Spiral-Wound LNG Heat Exchanger[J]. *ACS Omega*, **2023,** *8,* 11310−11317. Copyright [2023] American Chemical Society).

the raw gas gasification and compression, precooling compression, and cryogenic compression modules. In the experimental process, the precooling and cryogenic heat transfer parts of the double-mixed refrigerant system were placed on a sloshing platform for the relevant sloshing experiments. A flow chart is shown in Figure 3, where the heat transfer performance of the cryogenic heat transfer module is higher. A spiral-wound heat exchanger was selected to test the performance. A plate-fin heat exchanger was used in the precooling heat transfer module.

The actual device diagram corresponding to the above process is shown in Figure 4: Figure 4a is the overall diagram of the experimental device, and Figure 4b shows the heat exchanger sloshing platform. The LNG liquefaction sloshing experimental device included three small crowbars: heat transfer, refrigerant compression, and raw gas compression crowbars. Stainless-steel pipes were used to connect all parts of the crowbar. To facilitate installation, a hose connection was used between the heat transfer and raw compression crowbars.

https://doi.org/10.1021/acsomega.3c02983
ACS Omega 2023, 8, 27467−27481

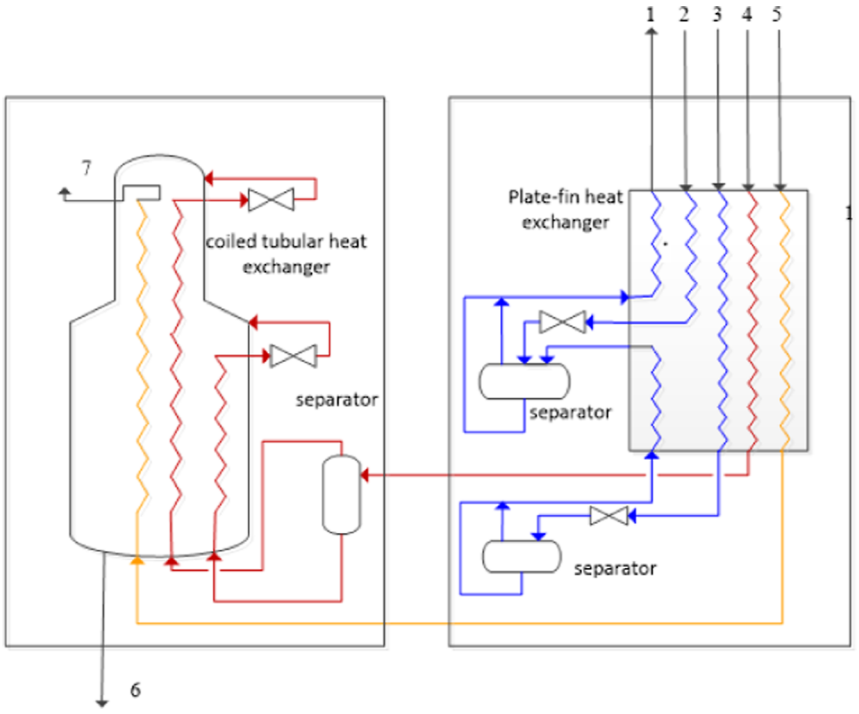

Figure 3. Cooling module flowchart (reproduced from Dong L F, Wu X, Liu K, Sun Q C. Influence of Sloshing Conditions on the Pressure Drop and Heat Transfer of a Single-Layer Spiral-Wound LNG Heat Exchanger[J]. *ACS Omega,* **2023,** *8,* 11310−11317. Copyright [2023], American Chemical Society).

(a) Overall device diagram (b) Experimental table of heat exchangers

Figure 4. (a) Overall device diagram (b) experimental table of heat exchangers. Experimental apparatus (reproduced from Dong L F, Wu X, Liu K, Sun Q C. Influence of Sloshing Conditions on the Pressure Drop and Heat Transfer of a Single-Layer Spiral-Wound LNG Heat Exchanger[J]. *ACS Omega,* **2023,** *8,* 11310−11317. Copyright [2023], American Chemical Society).

In the sloshing experiment, the heat-transfer crowbar was placed on the experimental platform and arranged reasonably according to the principle of weight balance.[23,24]

To calculate the heat transfer coefficient and pressure drop of the heat exchanger, the key geometric parameters of the equipment are listed in Table 1. The component of feed gas and shell-side refrigerant of the spiral-wound heat exchanger is shown in Table 2.

2.2. Measurement Deviation. The deviation is composed of system deviation and accidental deviation. Accidental deviation can be eliminated by increasing the average number of measurements. System deviation is mainly caused by the accuracy of the measuring instrument. Therefore, the influence of the deviation caused by the accuracy of the measuring instrument on the data analysis results is mainly analyzed.

2.2.1. Temperature Sensor Calibration and Deviation Correction. In order to ensure the authenticity and reliability of the experimental data, the temperature sensor is calibrated. The deviation of the temperature sensor in the normal temperature section is about ±0.5 °C. The temperature sensor in the low-temperature section is calibrated according to the professional institutions of the Aerospace Science and Industry Group at low temperatures. As shown in Table 3 and Table 4, the maximum measurement deviation of the low-temperature sensor before correction is about ±3.036%, the maximum deviation after correction is ±0.319%, and the minimum deviation is only ±0.0059%. Through deviation correction in the central control system, the accuracy of low-temperature acquisition is improved.

2.2.2. Data Calculation and Deviation Analysis. The deviation is composed of system deviation and accidental deviation. Accidental deviation can be eliminated by increasing

Table 1. Geometric Parameters of the Spiral Wound Heat Exchanger

parameter	value
vessel external diameter	8 mm
axial distance	13.2 mm
longitudinal distance	10.2 mm
core diameter	158 mm
shell-side diameter	309 mm
height of test exchanger	2910 mm
heated area	3.6 m^2

Table 2. Component of Feed Gas and Shell-Side Refrigerant of Spiral Wound Heat Exchanger

component	N_2	CH_4	C_2H_6	C_2H_4	C_3H_8	i-C_4H_{10}	n-C_4H_{10}
feed gas	0	83.5	10.6	0	4.5	0.4	0.1
shell-side refrigerant	5.1	59.9	4.6	29.5	0.4	0.3	0.3

https://doi.org/10.1021/acsomega.3c02983
ACS Omega 2023, 8, 27467−27481

Table 3. Calibration Correction of −100 °C Temperature Sensor Deviation

actual value	measured deviation	corrected deviation
−80	1.31	0.011958
−60	1.67	−0.01654
−50	1.9	0.018264
−30	2.21	−0.05928
−20	2.5	0.034379
0	2.86	0.005886

Table 4. Calibration Correction of −200 °C Temperature Sensor Deviation

actual value	measured deviation	corrected deviation
−196	0.162256	0.16532
−80	1.863043	−0.25924
−60	2.156282	−0.15402
−40	2.449522	−0.06852
−10	2.88938	−0.00924
0	3.036	0.319318

the average number of measurements. System deviation is mainly caused by the accuracy of the measuring instrument. Therefore, the influence of the deviation caused by the accuracy of the instrument on the experimental data analysis is mainly analyzed.

During the experiment, due to the influence of other factors such as the accuracy of the measuring instrument, in order to solve the problem of deviation synthesis, we must first clarify the functional relationship between indirect measurement and single measurement and then perform differential calculations according to the functional relationship between them.

Generally, the deviation can be considered in three aspects: the instrument deviation value given on the instrument instruction; the accuracy level of the instrument, which is determined by the range; and the minimum indexing value or half of the minimum indexing value.

3. STATIC EXPERIMENTAL ANALYSIS

The heat transfer coefficient U is an important parameter for measuring the heat transfer effect of the heat exchanger. For the same set of devices, the heat transfer area A was a constant value. Therefore, the UA value was used as an index to evaluate the heat transfer efficiency of the heat exchanger.

$$Q = c \cdot m \cdot \Delta t + Q_l \tag{1}$$

$$\mathrm{UA} = \frac{Q}{\mathrm{LMTD}} \tag{2}$$

$$\mathrm{LMTD} = \frac{|T_1 - t_2| - |T_2 - t_1|}{\ln \frac{T_1 - t_2}{T_2 - t_1}} \tag{3}$$

where U is the heat transfer coefficient, $W \cdot (m^2 \cdot K)^{-1}$; A is the heat exchange area, m^2; Q is the heat transfer rate, W; c is the specific heat capacity of the shell-side fluid, $J \cdot (kg \cdot K)^{-1}$; m is the mass flow of the shell-side fluid, $kg \cdot s^{-1}$; Q_l is the latent heat of the shell-side fluid, W; LMTD is the temperature difference between shell-side fluid and tube-side fluid, °C; T_1 and T_2 are the inlet and outlet temperatures of the shell-side fluid, °C; and t_1 and t_2 are the inlet and outlet temperatures of the tube-side fluid, °C.

Figure 5 shows the correlation between the UA value calculated by the static experiment and the UA value calculated by the two-phase heat transfer model developed by Neeraas[2] (eq 4). It can be observed that a large deviation of nearly 60% exists between the UA value obtained by the shell-side two-phase flow heat transfer model and the experimental value; therefore, the calculation model was not applicable.

The heat transfer coefficient is given as

$$U = a \cdot \left[\frac{2 \cdot \lambda^2 \cdot \rho^{4/3} \cdot g^{2/3} \cdot c_p}{\pi \cdot d_0 \cdot \mu^{1/3}}\right]^{1/3} \cdot \left[\frac{4 \cdot \Gamma}{\mu}\right]^b \tag{4}$$

If $Re < 2000$, $a = 0.886$, $a_1 = 0.762$, $b = 1/9$, $c = -1/3$, and $b = 1/3$. If $Re > 2000$, $a = 0.313$, $a_1 = 0.269$, $b = 1/4$, $c = -1/3$, and $b = 1/3$.

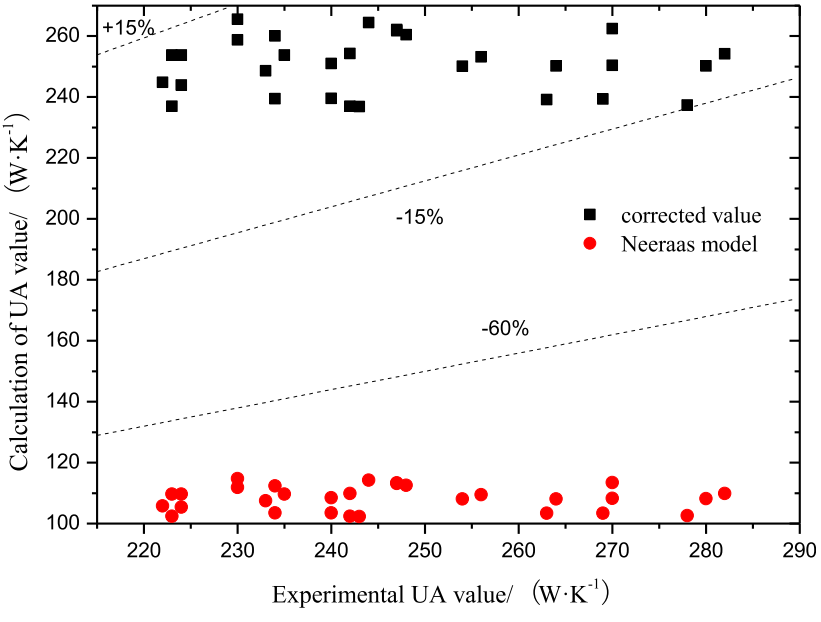

Figure 5. Comparison of the measured and calculated values.

https://doi.org/10.1021/acsomega.3c02983
ACS Omega 2023, 8, 27467−27481

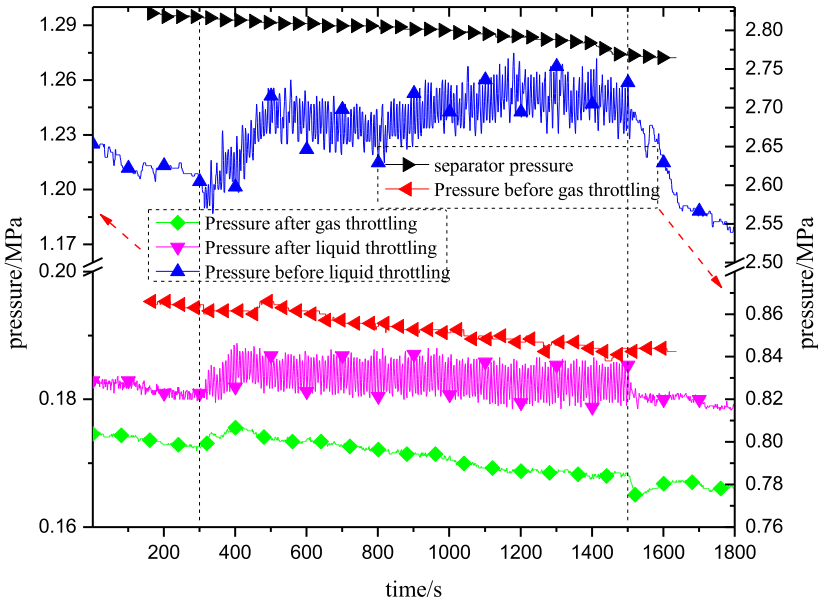

Figure 6. Pressure curve graph of spiral-wound heat exchangers.

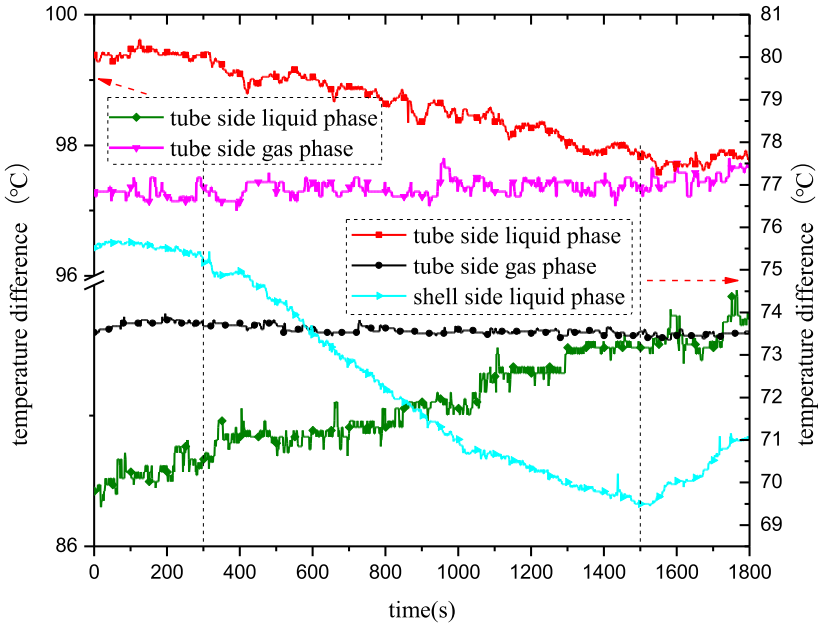

Figure 7. Temperature curve graph of spiral-wound heat exchangers.

Here, U is the heat transfer coefficient, $W\cdot(m^2\cdot K)^{-1}$; λ is the thermal conductivity of fluid, $W\cdot(m\cdot K)^{-1}$; ρ is the density of fluid, $kg\bullet m^{-3}$; c_p is the specific heat capacity of the fluid, $J\cdot(kg\cdot K)^{-1}$; g is the gravitational constant, $g = 9.8\ N\bullet kg^{-1}$; d_0 is the diameter of heat exchange tube, m; μ is viscosity of fluid, Pa•s; and Γ is the mass flow rate per unit length, $kg\cdot s^{-1}\cdot m^{-1}$. After the analysis, the heat transfer model was modified; the modified correlation is shown in eq 5. In this paper, 30 groups of experiments were carried out under static conditions, and the flow rate of natural gas ranged from 11.3 to 23.61 kg/h. The shell-side heat transfer coefficient measured by the experiment was compared with the calculated values of the Neeraas model and modified model. It can be observed from Figure 5 that the deviation between the corrected and experimental results is small and is controlled within 15%. Therefore, this correlation is applicable to the calculation of the shell-side heat transfer coefficient under the condition of mixed refrigerants for $1000 < Re < 2500$.

$$U^* = a\cdot\left[\frac{2\cdot\lambda_v^{\ 2}\cdot\rho_v^{\ 4/3}\cdot g_v^{\ 2/3}\cdot c_{pv}}{\pi\cdot d_0\cdot\mu_v^{\ 1/3}}\right]^{1/3}\cdot\left[\frac{\mu_l}{\mu_v}\right]^{1/4}\cdot\left[\frac{4\cdot\Gamma}{\mu_v}\right]^{b} \quad (5)$$

If $Re < 2000$, $a = 0.886$, and $b = 1/9$. If $Re > 2000$, $a = 0.313$, and $b = 1$, where subscript v is the vapor phase and l is the liquid phase.

4. ANALYSIS OF THE SLOSHING EXPERIMENT

4.1. Influence of the Sloshing Amplitude. To study the influence of the sloshing amplitude on the motion form of pitch, the sloshing amplitude and period were set as 3° and 10 s, 5° and 10 s, 7° and 10 s, and 9° and 10 s. The duration of

https://doi.org/10.1021/acsomega.3c02983
ACS Omega 2023, 8, 27467−27481

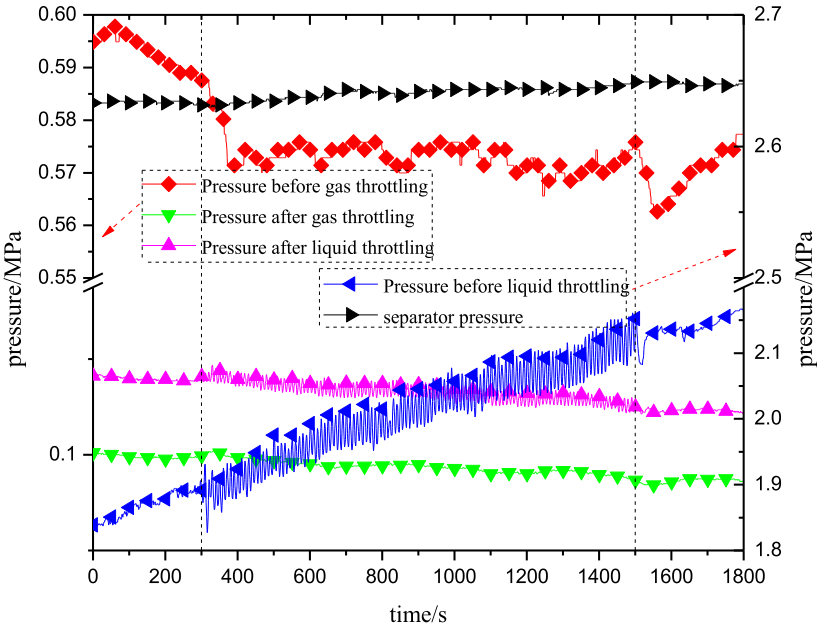

Figure 8. Pressure curve graph of spiral-wound heat exchangers.

the experiment was 20 min. The sloshing platform was still 5 min before and 5 min after the experiment.

4.1.1. Influence of a Pitch of 3° and a Period of 10 s. Figure 6 shows the pressure influence curve of the tubular heat exchanger. It can be seen from the diagram that during the sloshing experiment, the pressure fluctuation trend before and after the liquid throttling was consistent with the motion trend of the sloshing platform. The motion trend is a sine curve with a change period of 10 s. The pressure fluctuation value and fluctuation amplitude before and after gas throttling were 0.0234 MPa and 2.75%, and 0.0081 MPa and 4.71%, respectively. The pressure fluctuation value and fluctuation amplitude before and after liquid throttling were 0.088 MPa and 7.10%, and 0.0103 MPa and 5.60%, respectively. This is due to the device in the sloshing condition: when the platform moves to the highest point when the speed was 0 m•s^{-1}, the acceleration was large, and the deep refrigerant in the pipeline produced a large centrifugal force; when the platform moved to the initial position, the velocity reached a maximum, but because the acceleration direction was perpendicular to the velocity, which was 0 m•s^{-2}, the cryogenic refrigerant was not subjected to centrifugal force.

Figure 7 shows the influence curve of the temperature difference in the tube heat exchanger. It can be seen from the diagram that the liquid temperature difference on the shell side decreased with an increase in sloshing time during the sloshing experiment. When the sloshing stopped, the liquid temperature difference on the shell side increased gradually. This was due to the liquid film distribution when the liquid refrigerant dropped through the distributor, and the existence of sloshing conditions, resulting in liquid film rupture, which exposed some heat exchange tubes, weakening the heat transfer capacity. The fluctuation value of the temperature difference between the inlet and outlet of the liquid refrigerant in the pipeline was 2.466 °C, and the fluctuation range was 3.13%. The fluctuation of the temperature difference between the inlet and outlet of the gas refrigerant was 0.415 °C, and the fluctuation range was 0.56%. The fluctuation value of the temperature difference between the inlet and outlet of the shell-side liquid refrigerant was 5.934 °C, the fluctuation range was 8.25%, the fluctuation of the temperature difference between the inlet and outlet of the shell-side gas refrigerant was 1.026 °C, and the fluctuation range was 1.18%. The temperature fluctuation of the inlet and outlet pipes of the raw gas was 0.806 °C, and the fluctuation range was 0.83%. It can be observed that the fluctuation amplitude of the liquid refrigerant was far greater than that of the gas refrigerant. This is because, when the gas and liquid refrigerants moved at the same acceleration, the density of the liquid refrigerant was large, which resulted in a high centrifugal force. As a result, the fluctuation was large.

4.1.2. Influence of a Pitch of 5° and a Period of 10 s. Figure 8 shows the pressure influence curve of the spiral-wound heat exchanger. The value and amplitude of pressure fluctuation are shown in Table 5. This is because for a device

Table 5. Pressure Fluctuation Value and Amplitude

	before gas throttling	after gas throttling	before liquid throttling	after liquid throttling
fluctuation value (MPa)	0.022	0.015	0.334	0.025
fluctuation amplitude (%)	3.83	15.899	16.61	18.72

subjected to sloshing conditions, when the platform moves to the highest point when the speed is 0 m·s^{-1}, the acceleration is large, and the deep refrigerant in the pipeline produces a large centrifugal force. When the platform moves to the initial position, the velocity reaches its maximum value, but because the acceleration direction is perpendicular to the velocity, which is 0 m·s^{-2}, the cryogenic refrigerant is not subjected to a centrifugal force.

Figure 9 shows the influence curve of the temperature difference in the heat exchanger. It can be seen from the diagram that the liquid temperature difference on the shell side decreased with an increase in sloshing time during the sloshing experiment. When the sloshing stopped, the liquid temperature difference on the shell side gradually increased. This is due to

https://doi.org/10.1021/acsomega.3c02983
ACS Omega 2023, 8, 27467−27481

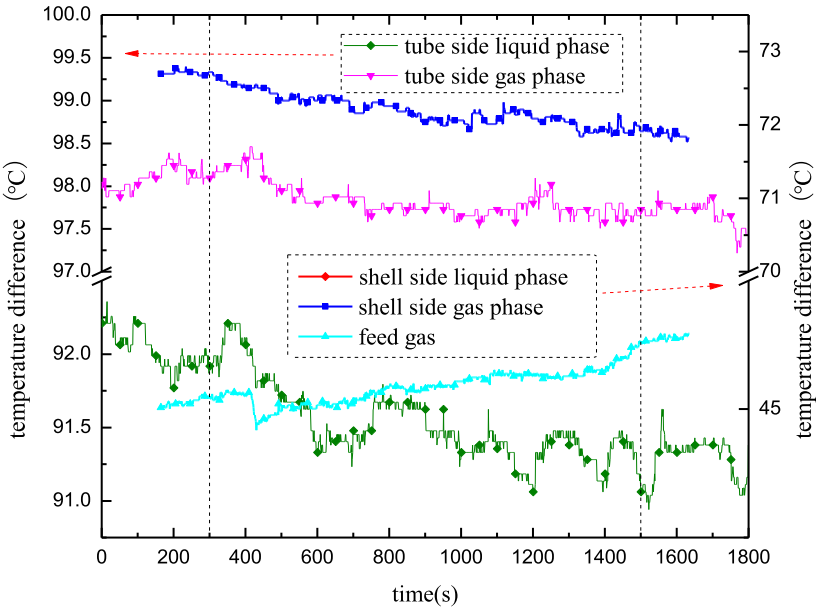

Figure 9. Temperature curve graph of spiral-wound heat exchangers.

the liquid film distribution when the liquid refrigerant drops through the distributor, and the existence of sloshing conditions, which result in liquid film rupture, exposing some heat exchange tubes and weakening the heat transfer capacity. The value and amplitude of temperature fluctuation are shown in Table 6.

Table 6. Temperature Fluctuation Value and Amplitude

	liquid refrigerant on the tube side	gas refrigerant in the pipeline	shell-side liquid refrigerant	shell-side gas refrigerant	raw gas
fluctuation value (°C)	0.757	0.708	1.245	1.148	0.952
fluctuation amplitude (%)	1.18	0.98	2.74	1.25	0.97

4.1.3. Influence of a Pitch of 7° and a Period of 10 s. Figure 10 shows the pressure variation curves of the spiral-wound heat exchanger. It can be seen that the pressure before throttling of liquid refrigerant, the pressure after throttling of the gas phase, and the pressure after throttling of the liquid phase all increased first and then decreased slowly. This is because, for a device subjected to sloshing conditions, when the speed is 0 $m \cdot s^{-1}$, the acceleration is large, and the deep refrigerant in the pipeline produces a large centrifugal force; when the velocity reaches a maximum, the acceleration direction is perpendicular to the velocity, which is 0 $m \cdot s^{-2}$. The centrifugal force on the cryogenic agent is 0. The value and amplitude of pressure fluctuation are shown in Table 7.

Figure 11 shows the curve of the temperature difference in the heat exchanger. It can be seen that the liquid-phase temperature difference and gas-phase temperature difference decreased with the increase in sloshing time during the sloshing experiment, and the temperature difference increased gradually when the sloshing stopped. This is because the liquid refrigerant formed a layer of liquid film on the surface of the heat exchange tube when the refrigerant dropped through the distributor, and the liquid film ruptured because of the

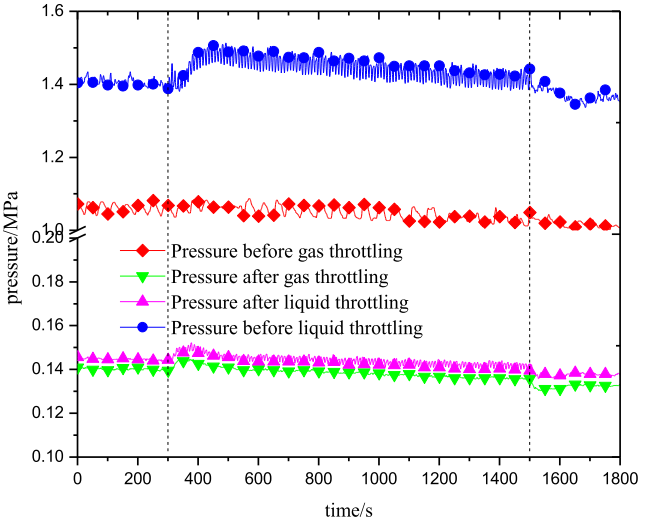

Figure 10. Pressure curve graph of spiral-wound heat exchangers.

Table 7. Pressure Fluctuation Value and Amplitude

	before gas throttling	after gas throttling	before liquid throttling	after liquid throttling
fluctuation value (MPa)	0.078	0.009	0.138	0.012
fluctuation amplitude (%)	7.40	6.69	9.53	8.46

existence of sloshing conditions, which exposed some heat exchange tubes and weakened the heat transfer capacity. The value and amplitude of temperature fluctuation are shown in Table 8.

4.1.4. Influence of a Pitch of 9° and a Period of 10 s. Figure 12 shows the pressure variation curve for the tubular heat exchanger. It can be observed that the pressure fluctuation trends of the gas and liquid refrigerants were consistent before throttling. When sloshing started, the pressure increased, and when sloshing ended, the pressure decreased. The pressure fluctuation trends of the gas-phase refrigerant and liquid-phase

https://doi.org/10.1021/acsomega.3c02983
ACS Omega 2023, 8, 27467−27481

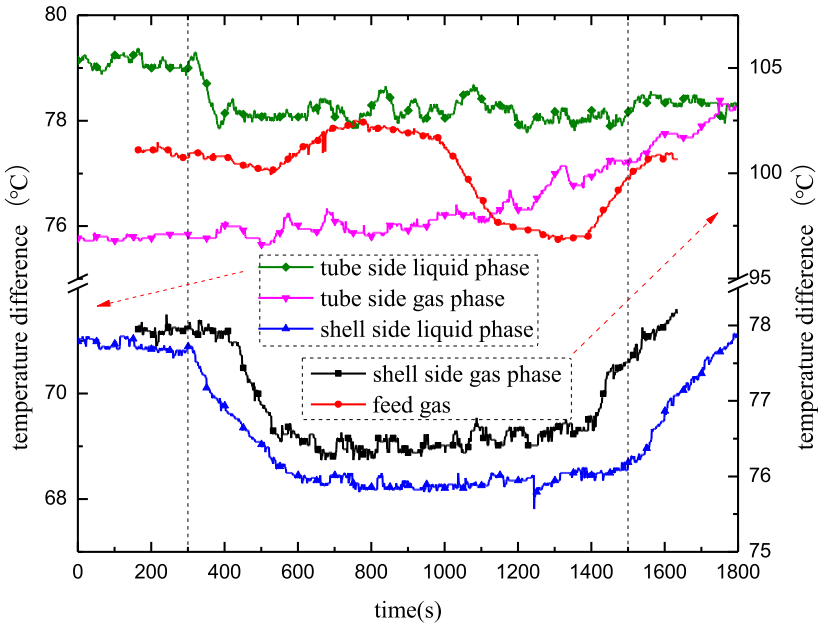

Figure 11. Temperature curve graph of spiral-wound heat exchangers.

Table 8. Temperature Fluctuation Value and Amplitude

	liquid refrigerant on the tube side	gas refrigerant in the pipeline	shell-side liquid refrigerant	shell-side gas refrigerant	raw gas
fluctuation value (°C)	1.514	1.636	3.077	1.709	5.651
fluctuation amplitude (%)	1.94	2.15	4.48	2.23	5.64

refrigerant were consistent after throttling, and the pressure first increased and then decreased during the sloshing experiment. The value and amplitude of pressure fluctuation are shown in Table 9.

Table 9. Pressure Fluctuation Value and Amplitude

	before gas throttling	after gas throttling	before liquid throttling	after liquid throttling
fluctuation value (MPa)	0.089	0.023	0.207	0.021
fluctuation amplitude (%)	8.53	15.786	9.71	15.35

Figure 13 shows the curve of the temperature difference in the heat exchanger. It can be seen from the diagram that the liquid temperature difference on the shell side decreased with an increase in sloshing time during the sloshing experiment. When sloshing stopped, the liquid temperature difference on the shell side increased gradually. This is due to the liquid film distribution when the liquid refrigerant drops through the distributor, and the existence of sloshing conditions, resulting

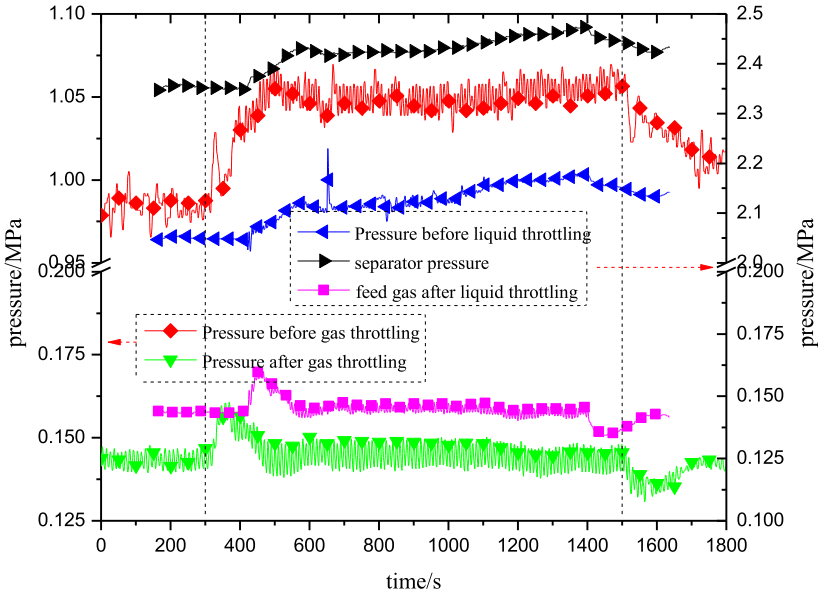

Figure 12. Pressure curve graph of spiral-wound heat exchangers.

https://doi.org/10.1021/acsomega.3c02983
ACS Omega 2023, 8, 27467−27481

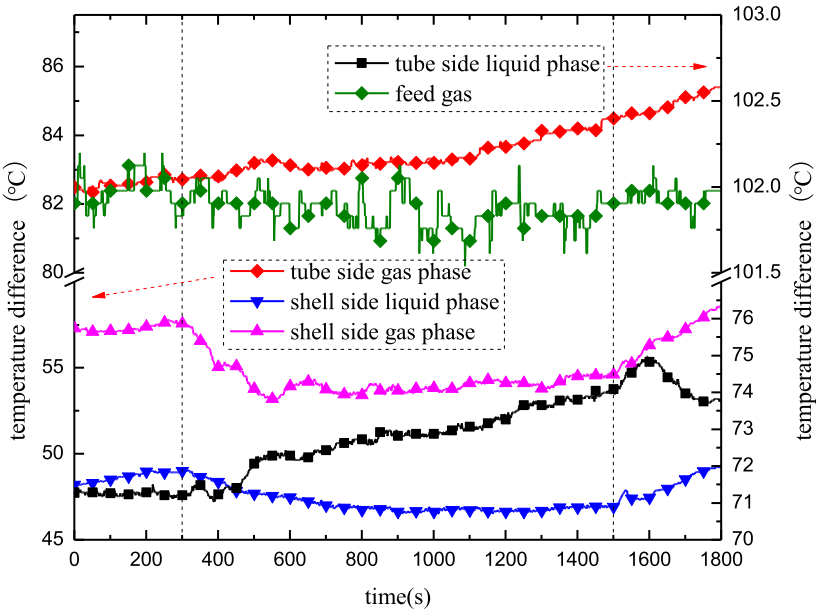

Figure 13. Temperature curve graph of spiral-wound heat exchangers.

in liquid film rupture, which exposes some heat exchange tubes, weakening the heat transfer capacity. The value and amplitude of temperature fluctuation are shown in Table 10.

Table 10. Temperature Fluctuation Value and Amplitude

	liquid refrigerant on the tube side	gas refrigerant in the pipeline	shell-side liquid refrigerant	shell-side gas refrigerant	raw gas
fluctuation value (°C)	3.053	1.831	2.564	4.469	0.586
fluctuation amplitude (%)	4.20	2.20	5.44	8.23	0.58

4.1.5. Summary of Results. By combining the different sloshing conditions, it was found that sloshing affects the uniformity of the refrigerant on the shell side of the tube-round heat exchanger, thus affecting the heat transfer effect of the heat exchanger. Figure 14 shows the variation curve of the UA value with time under different sloshing amplitudes. It can be observed that when the sloshing angle is 3°, the UA value increases slowly with sloshing, which is 12.92% higher than the average value. When the sloshing amplitude was 5−9°, the UA values decreased to varying degrees. Among them, the UA value of 5° pitch decreased by 38.12%; the UA value of 7° pitch decreased by 40.53%; and the UA value of 9° pitch decreased by 42.03%. It can be concluded that with an increase in the sloshing amplitude, the heat exchanger was more affected, and the heat transfer effect was reduced. This is because when sloshing is carried out at a small sloshing angle of 3°, the uniformity of the shell-side refrigerant in the heat exchanger and heat transfer performance of the heat exchanger is improved. However, with an increase in the sloshing angle, when the sloshing angle was greater than 5°, the liquid film of the shell-side refrigerant was separated from the heat exchange tube, resulting in insufficient heat transfer of the heat exchanger and weakening of the heat transfer effect of the heat exchanger.

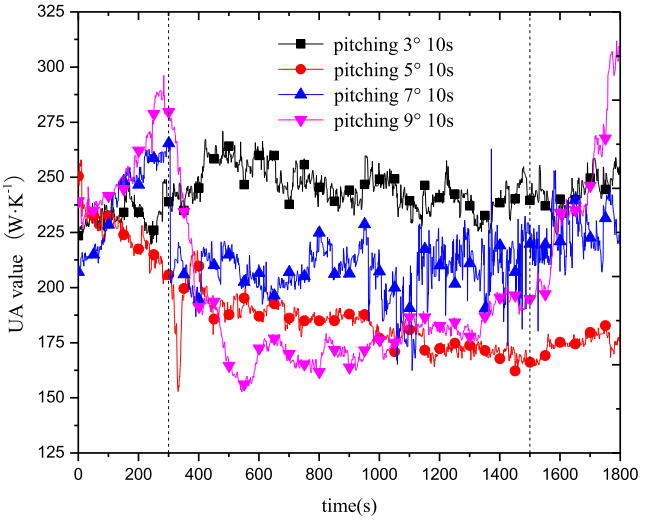

Figure 14. UA values of spiral-wound heat exchangers with respect to time.

For the same experimental device, the shell-side heat exchange tube area is certain; therefore, the fluctuation of the UA value is consistent with the heat transfer coefficient α. Figure 15 shows the deviation value of the heat transfer coefficient for different sloshing angles. It can be observed from the figure that the fitting curve is highly matched with the experimentally measured value. Therefore, in the form of pitch sloshing, the empirical correlation of the heat transfer coefficient with the sloshing angle is

$$U_{\text{pitch}} = U^{*}\cdot(1 + P) \tag{6}$$

$$P = P_0 + \left(\frac{a}{b\cdot\sqrt{\frac{\pi}{2}}}\right)\cdot e^{-2\left(\frac{\theta - c}{b}\right)^2} \tag{7}$$

where U_{pitch} is the heat transfer coefficient, $W\cdot(m^2\cdot K)^{-1}$; P is the deviation; and θ is the sloshing angle. $P_0 = -41.29$, $a = 303.06$, $b = 72.58$, and $c = 1.65$.

https://doi.org/10.1021/acsomega.3c02983
ACS Omega 2023, 8, 27467−27481

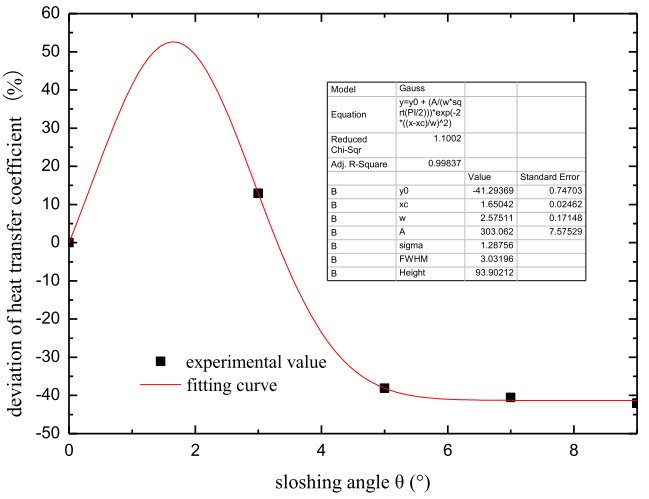

Figure 15. Deviation values of α at different sloshing angles.

4.2. Influence of the Sloshing Period. To study the influence of the sloshing period on the heat transfer performance, experiments were conducted with a sloshing amplitude of 5 °and sloshing periods of 6, 10, 15, and 20 s. The experiment lasted for a total of 20 min, and the platform was stationary for 5 min before and 5 min after the experiment, as in the experimental comparison.

4.2.1. Influence of a Pitch of 5° and a Period of 10 s. Figure 16 shows the pressure variation curve for the tubular heat exchanger. It can be seen that during the sloshing experiment, the pressure fluctuation trends of the gas-phase refrigerant and liquid-phase refrigerant before throttling were consistent. When sloshing started, the pressure increased, and when sloshing ended, the pressure decreased. The pressure fluctuation trends of the gas-phase refrigerant and liquid-phase refrigerant were consistent after throttling, and the pressure first increased and then decreased during the sloshing experiment. The value and amplitude of pressure fluctuation are shown in Table 11. This is because for the device subjected to sloshing conditions, when the platform moves to the highest point when the speed is 0 m·s^{-1}, the acceleration is large, and deep refrigerant in the pipeline produces a large centrifugal force; when the platform moves to the initial position, the velocity reaches a maximum, but because the acceleration direction is perpendicular to the velocity, which is 0 m·s^{-2}, the cryogenic refrigerant is not subjected to centrifugal force.

Table 11. Pressure Fluctuation Value and Amplitude

	before gas throttling	after gas throttling	before liquid throttling	after liquid throttling
fluctuation value (MPa)	0.076	0.024	0.095	0.020
fluctuation amplitude (%)	7.51	15.94	4.52	13.11

Figure 17 shows the influence curve of the temperature difference in the heat exchanger. It can be seen that the liquid temperature difference on the shell side decreased with an increase in the sloshing time. When sloshing stopped, the liquid temperature difference on the shell side increased gradually. This is due to the liquid film distribution when the liquid refrigerant drops through the distributor, and the existence of sloshing conditions, resulting in liquid film rupture, which exposes some heat exchange tubes, weakening the heat transfer capacity. The value and amplitude of temperature fluctuation are shown in Table 12.

4.2.2. Influence of a Pitch of 5° and a Period of 15 s. Figure 18 shows the pressure curves of the heat exchanger. It can be seen that during the sloshing experiment, the pressure fluctuation trends of the gas-phase refrigerant and liquid-phase refrigerant after throttling were consistent. When sloshing started, the pressure increased, and when sloshing ended, the pressure decreased. The pressure fluctuation trends of the gas-phase refrigerant before throttling decreased during the sloshing experiment. The value and amplitude of pressure fluctuation are shown in Table 13.

Figure 19 shows the influence curve of the temperature difference in the heat exchanger. It can be seen that the liquid temperature difference on the shell side decreased with an

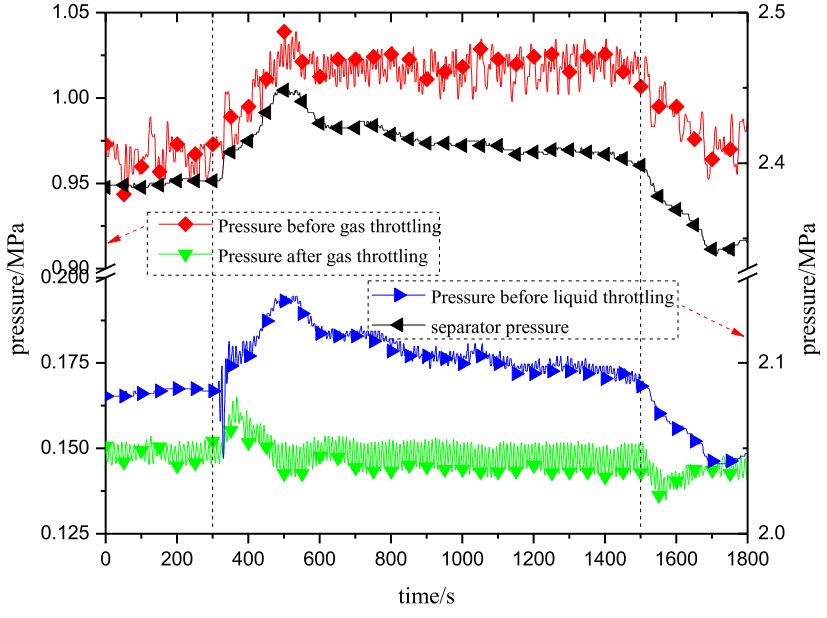

Figure 16. Pressure curve graph of spiral-wound heat exchangers.

https://doi.org/10.1021/acsomega.3c02983
ACS Omega 2023, 8, 27467−27481

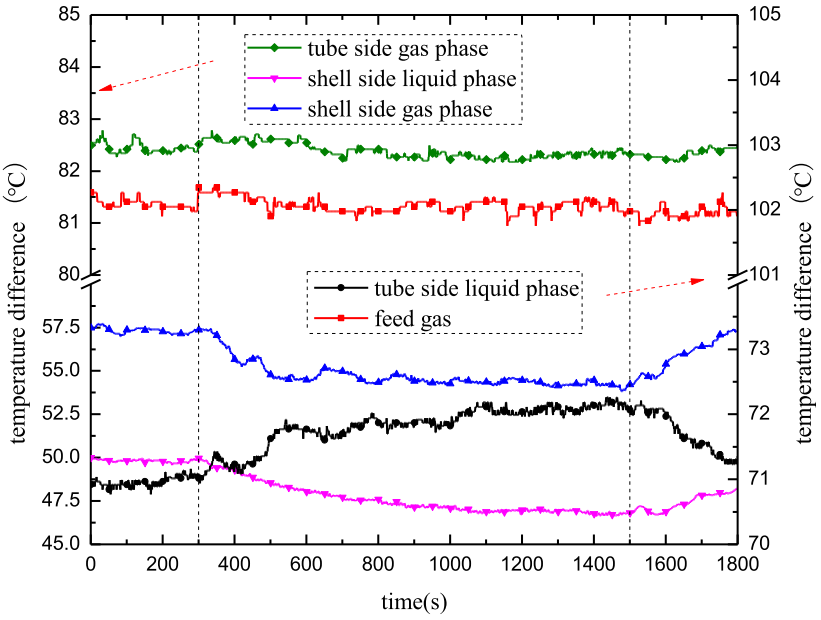

Figure 17. Temperature curve graph of spiral-wound heat exchangers.

Table 12. Temperature Fluctuation Value and Amplitude

	liquid refrigerant on the tube side	gas refrigerant in the pipeline	shell-side liquid refrigerant	shell-side gas refrigerant	raw gas
fluctuation value (°C)	1.319	0.610	3.346	3.614	0.586
fluctuation amplitude (%)	1.83	0.74	7.14	6.66	0.57

Table 13. Pressure Fluctuation Value and Amplitude

	before gas throttling	after gas throttling	before liquid throttling	after liquid throttling
fluctuation value (MPa)	0.070	0.017	0.362	0.023
fluctuation amplitude (%)	11.08	15.50	23.15	15.39

increase in the sloshing time. When sloshing stopped, the liquid temperature difference on the shell side increased gradually. This is due to the liquid film distribution when the liquid refrigerant drops through the distributor, and the existence of sloshing conditions, resulting in liquid film rupture, which exposes some heat exchange tubes, weakening the heat transfer capacity. The value and amplitude of temperature fluctuation are shown in Table 14.

4.2.3. Influence of a Pitch of 5° and a Period of 20 s. Figure 20 shows the pressure variation curve of the tubular heat exchanger. It can be seen that during the sloshing experiment, the pressure fluctuation trends of the gas-phase

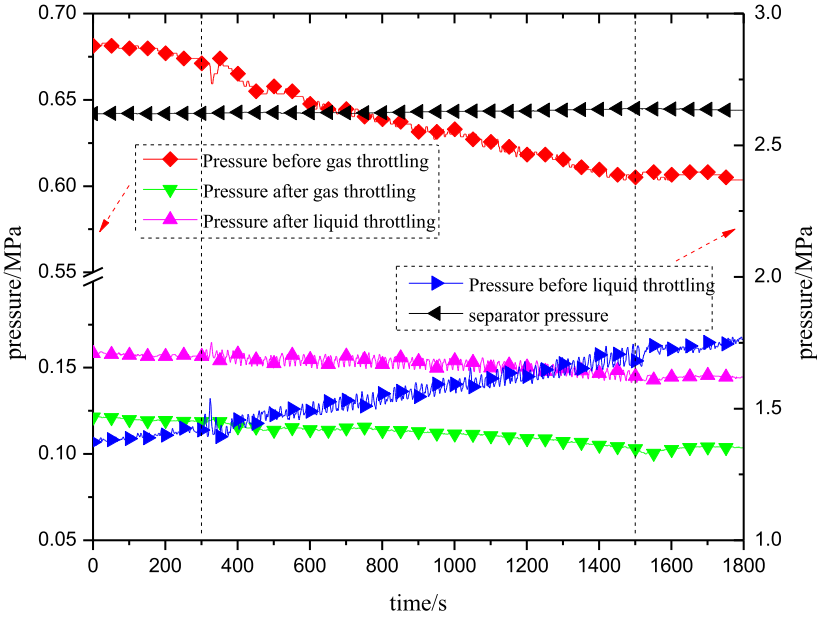

Figure 18. Pressure curve graph of spiral-wound heat exchangers.

https://doi.org/10.1021/acsomega.3c02983
ACS Omega 2023, 8, 27467−27481

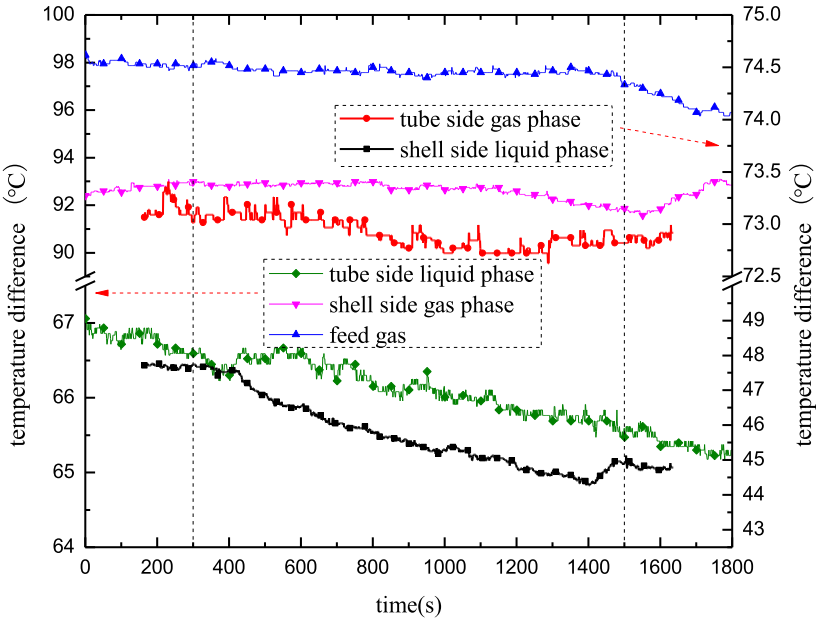

Figure 19. Temperature curve graph of spiral-wound heat exchangers.

Table 14. Temperature Fluctuation Value and Amplitude

	liquid refrigerant on the tube side	gas refrigerant in the pipeline	shell-side liquid refrigerant	shell-side gas refrigerant	raw gas
fluctuation value (°C)	1.197	0.635	3.248	1.368	1.172
fluctuation amplitude (%)	1.83	0.87	7.35	1.49	1.21

refrigerant and liquid-phase refrigerant after throttling were consistent. When sloshing started, the pressure increased, and when sloshing ended, the pressure decreased. The pressure fluctuation trends of the gas-phase refrigerant before throttling decreased during the sloshing experiment. The value and amplitude of pressure fluctuation are shown in Table 15.

Table 15. Pressure Fluctuation Value and Amplitude

	before gas throttling	after gas throttling	before liquid throttling	after liquid throttling
fluctuation value (MPa)	0.081	0.017	0.283	0.018
fluctuation amplitude (%)	11.33	12.69	22.43	10.96

Figure 21 shows the temperature difference curve in the heat exchanger. It can be seen that the liquid temperature difference on the shell side decreased with an increase in the sloshing time. When sloshing stopped, the liquid temperature difference

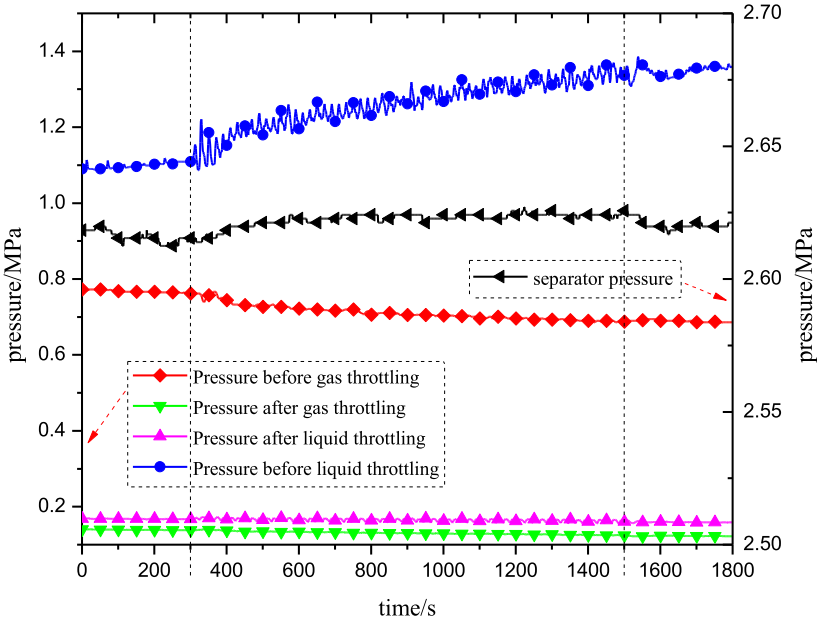

Figure 20. Pressure curve graph of spiral-wound heat exchangers.

https://doi.org/10.1021/acsomega.3c02983
ACS Omega 2023, 8, 27467−27481

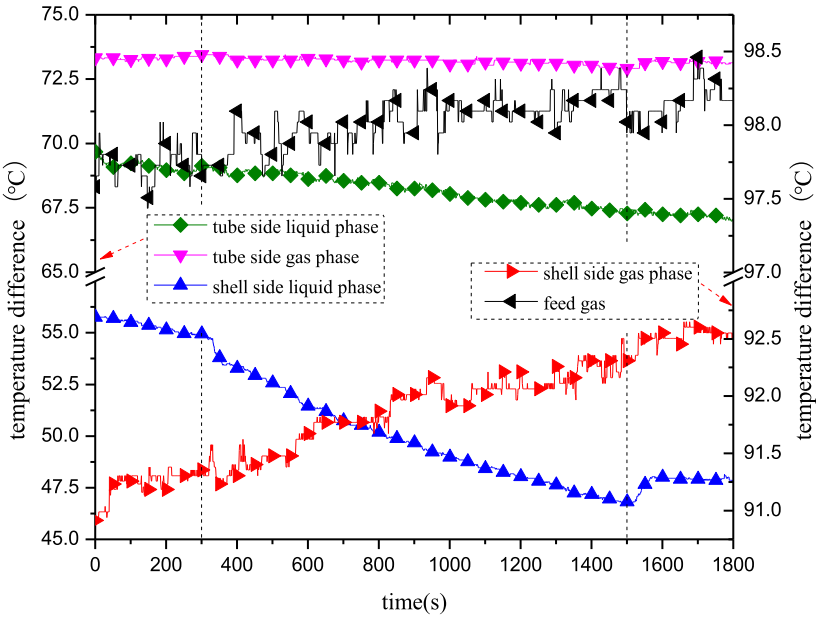

Figure 21. Temperature curve graph of spiral-wound heat exchangers.

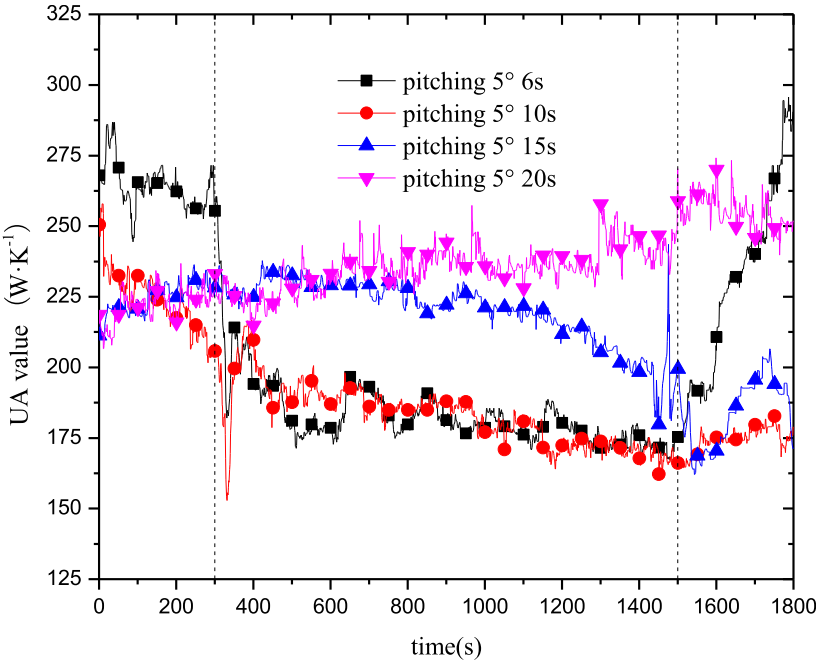

Figure 22. Variation in the UA value of spiral-wound heat exchangers with time.

on the shell side increased gradually. This is due to the liquid film distribution when the liquid refrigerant drops through the distributor, and the existence of sloshing conditions, resulting in liquid film rupture, which exposes some heat exchange tubes, weakening the heat transfer capacity. The temperature difference between the shell side and the inlet and outlet of the raw gas increased with sloshing, owing to the sloshing promoting contact between some working fluids and the heat exchange tube, which improved the heat transfer effect. The temperature difference between the inlet and outlet of the liquid refrigerant in the pipeline decreased by 2.79%, the temperature difference between the inlet and outlet of the gas refrigerant in the pipe decreased by 0.74%, the temperature difference between the inlet and outlet of the shell-side liquid refrigerant decreased by 17.53%, and the temperature difference between the inlet and outlet of the shell-side gas refrigerant increased by 1.38%. The temperature difference between the inlet and outlet of the raw gas increased by 0.75%.

4.2.4. Summary of Results. Figure 22 shows the variation curve of the UA value with time under different sloshing amplitudes. It can be observed that when the sloshing period was 20 s, the UA value increases slowly with the sloshing process, which was 10.82% higher than that at rest. When the sloshing amplitude was 6−15 s, the UA values decreased by varying degrees. The UA value decreased by 36.66% when the rolling period was 6 s. The UA value decreased by 35.00% when the rolling period was 10 s. The UA value decreased by 18.56% after 15 s. It can be concluded that, with a decrease in

https://doi.org/10.1021/acsomega.3c02983
ACS Omega 2023, 8, 27467−27481

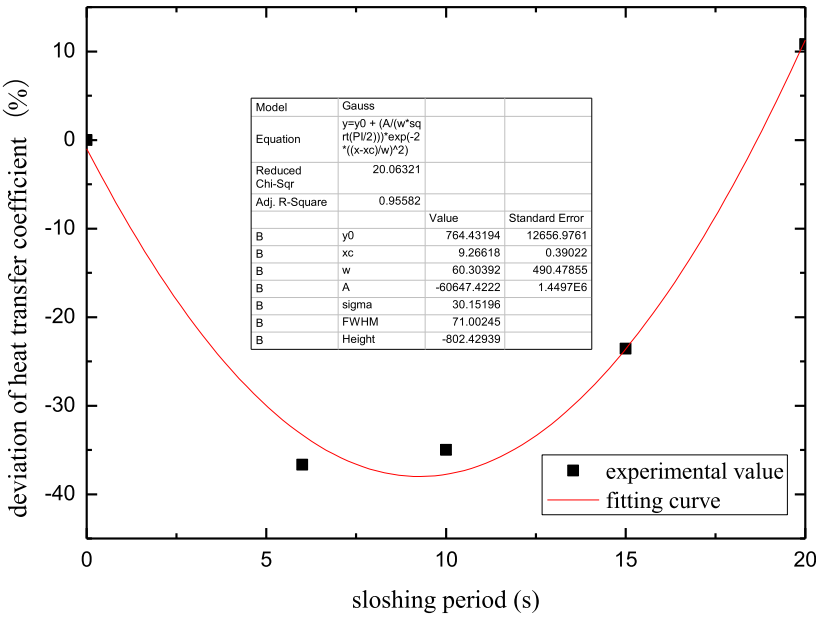

Figure 23. Deviation value of α at different sloshing periods.

the sloshing period, the heat exchanger was more affected, and the heat transfer effect was reduced. This is because when the sloshing period is 20 s, owing to the larger sloshing period, the linear velocity is smaller when the sloshing occurs, the uniform distribution characteristics of the shell-side refrigerant in the heat exchanger are improved, and the heat transfer performance of the heat exchanger is improved. However, with a decrease in the sloshing period, when the sloshing period was less than 10 s, the liquid film of the shell-side refrigerant was separated from the heat exchange tube in a large area, resulting in insufficient heat transfer in the heat exchanger and a weakening of the heat transfer effect of the heat exchanger.

Figure 23 shows the deviation value of the heat transfer coefficient for different sloshing periods. It can be observed from the figure that the fitting curve agrees with the experimentally measured values. Therefore, the empirical correlation of the heat transfer coefficient with the sloshing period is

$$U_{\text{pitch}} = U^{*}\cdot(1 + P) \tag{8}$$

$$P = P_0 + \left(\frac{a}{b\cdot\sqrt{\frac{\pi}{2}}}\right)\cdot e^{-2\left(\frac{T-c}{b}\right)^2} \tag{9}$$

where T is the sloshing period, s; P_0 = 764.432, a = 9.266, b = 60.304, and c = −60647.422.

5. RESULTS AND DISCUSSION

In this study, based on experimental data, a heat transfer model of the static heat exchanger was established. The model was then used to study the influence of different sloshing amplitudes and periods on the heat transfer performance of the heat exchanger under the condition of longitudinal sloshing. The following conclusions can be drawn:

(1) The fluctuation of the UA value first increased and then decreased with an increase in the sloshing amplitude. The UA value at a 3° pitch was 12.92% higher than the average value; at a 9° pitch, it decreased by 42.03%.

(2) The fluctuation of the UA value first decreased and then increased with an increase in the sloshing period. The UA value was 36.66% lower than the average value when the sloshing period was 6 s; it increased by 10.82% slowly when the sloshing period was 20 s.

(3) Based on the experimental data, mathematical heat transfer models with different sloshing amplitudes and periods were established.

AUTHOR INFORMATION

Corresponding Author

Longfei Dong − *Shandong Institute of Petroleum and Chemical Technology, Dongying, Shandong 257061, China;* orcid.org/0000-0001-5106-2541; Email: dlf_upc@163.com

Authors

Hao Wang − *Shandong Institute of Petroleum and Chemical Technology, Dongying, Shandong 257061, China*

Xiao Wu − *Shandong Institute of Petroleum and Chemical Technology, Dongying, Shandong 257061, China;* orcid.org/0000-0001-7803-740X

Yanping Xin − *Shandong Institute of Petroleum and Chemical Technology, Dongying, Shandong 257061, China*

Shunyao Jiang − *Shandong Institute of Petroleum and Chemical Technology, Dongying, Shandong 257061, China*

Hailei Yao − *Shandong Institute of Petroleum and Chemical Technology, Dongying, Shandong 257061, China*

Yanling Huo − *Shandong Institute of Petroleum and Chemical Technology, Dongying, Shandong 257061, China*

Complete contact information is available at: https://pubs.acs.org/10.1021/acsomega.3c02983

Notes

The authors declare no competing financial interest.

ACKNOWLEDGMENTS

This work was supported by the Science Development Funding Program of Dongying of China (grant no.

https://doi.org/10.1021/acsomega.3c02983
ACS Omega 2023, 8, 27467−27481

DJ2021009) and the Science Development Funding Program of Dongying of China (grant no. DJ2021008).

REFERENCES

(1) Neeraas, B. O.; Fredheim, A. O.; Aunan, B. Experimental shell-side heat transfer and pressure drop in gas flow for spiral-wound LNG heat exchanger. *Int. J. Heat Mass Transfer* **2004**, *47*, 353−361.
(2) Neeraas, B. O.; Fredheim, A. O.; Aunan, B. Experimental data and model for heat transfer, in liquid falling film flow on shell-side, for spiral-wound LNG heat exchanger. *Int. J. Heat Mass Transfer* **2004**, *47*, 3565−3572.
(3) Li, J. R.; Chen, J.; Pu, H.; et al. Simulation of falling film flow and heat transfer at shell-side of coil-wound heat exchanger[J]. *CIESC J.* **2015**, *66*, 40−49.
(4) Li, J.; Hu, H.; Wang, H. Numerical investigation on flow pattern transformation and heat transfer characteristics of two-phase flow boiling in the shell side of LNG spiral wound heat exchanger. *Int. J. Therm. Sci.* **2020**, *152*, 106289.
(5) Genic, S. B.; Jacimovic, B. M.; Jaric, M. S.; Budimir, N. J.; Dobrnjac, M. M. Research on the shell-side thermal performances of heat exchangers with helical tube coils. *Int. J. Heat Mass Tran.* **2012**, *55*, 4295−4300.
(6) Abolmaali, A. M.; Afshin, H. Numerical study of heat transfer between shell-side fluid and shell wall in the spiral-wound heat exchangers. *Int. J. Refrig.* **2020**, *120*, 285−295.
(7) Jian, G.; Peterson, G. P.; Wang, S. Experimental investigation of the condensation mechanisms in the shell side of spiral wound heat exchangers. *Int. J. Heat Mass Transfer* **2020**, *154*, 119733.
(8) Zheng, W.; Jiang, Y.; Wang, Y.; Li, F.; Cui, Q. Distribution characteristics of liquid in spiral-wound heat exchanger under sloshing conditions. *J. Therm. Anal. Calorim.* **2020**, *141*, 587−598.
(9) Sharqawy, M. H.; Saad, S. M. I.; Ahmed, K. K. Effect of flow configuration on the performance of spiral-wound heat exchanger[J]. *Appl. Therm. Eng.* **2019**, *161*, 114157−114186.
(10) Hu, H.; Ding, C.; Ding, G.; Chen, J.; Mi, X.; Yu, S. Heat transfer characteristics of two-phase mixed hydrocarbon refrigerants flow boiling in shell side of LNG spiral wound heat exchanger. *Int. J. Heat Mass Transfer* **2019**, *131*, 611−622.
(11) Tang, Q. X.; Chen, G. F.; Yang, Z. Q.; Shen, J.; Gong, M. Numerical investigation on gas flow heat transfer and pressure drop in the shell side of spiral-wound heat exchangers. *Sci. China Technol. Sci.* **2018**, *61*, 506−515.
(12) Zeng, M.; Zhang, G.; Li, Y.; Niu, Y.; Ma, Y.; Wang, Q. Geometrical Parametric Analysis of Flow and Heat Transfer in the Shell Side of a Spiral-Wound Heat Exchanger. *Heat Transfer Eng.* **2015**, *36*, 790−805.
(13) Lu, X.; Du, X.; Zeng, M.; Zhang, S.; Wang, Q. Shell-side thermal-hydraulic performances of multilayer spiral-wound heat exchangers under different wall thermal boundary conditions. *Appl. Therm. Eng.* **2014**, *70*, 1216−1227.
(14) Li, Y. X.; Liu, L.; Wang, S. W.; et al. Research on numerical simulation of heat transfer of falling film flow in FLNG spiral-wound heat exchanger under rolling conditions[J]. *China Offshore Oil Gas* **2021**, *1*, 184−191.
(15) Ren, Y.; Cai, W.; Jiang, Y. Numerical study on shell-side flow and heat transfer of spiral-wound heat exchanger under sloshing working conditions. *Appl. Therm. Eng.* **2018**, *134*, 287−297.
(16) Ren, Y.; Cai, W.; Chen, J.; Lu, L.; Jiang, Y. Numerical study on the shell-side flow and heat transfer of superheated vapor flow in spiral wound heat exchanger under rolling working conditions. *Int. J. Heat Mass Transfer* **2018**, *121*, 691−702.
(17) Ren, Y.; Cai, W.; Chen, J.; Lu, L.; Wang, J.; Jiang, Y. The heat transfer characteristic of shell-side film flow in spiral wound heat exchanger under rolling working conditions. *Appl. Therm. Eng.* **2018**, *132*, 233−244.
(18) Sun, C.; Li, Y.; Zhu, J.; Han, H. Experimental tube-side pressure drop characteristics of FLNG spiral wound heat exchanger under sloshing conditions. *Exp. Therm. Fluid Sci.* **2017**, *88*, 194−201.
(19) Sun, C.; Li, Y.; Han, H.; Zhu, J.; Wang, S. Effect of compound sloshing conditions on pressure drop and heat transfer characteristics for FLNG spiral wound heat exchanger. *Appl. Therm. Eng.* **2019**, *159*, 113791−113810.
(20) Wang, T.; Ding, G.; Ren, T.; Chen, J.; Pu, H. A mathematical model of floating LNG spiral-wound heat exchangers under rolling conditions. *Appl. Therm. Eng.* **2016**, *99*, 959−969.
(21) Zheng, W.; Jiang, Y.; Wang, Y. The sloshing effects on distribution characteristics of gas−liquid mixture in spiral-wound heat exchanger. *J. Therm. Anal. Calorim.* **2020**, *141*, 599−612.
(22) Duan, Z.; Ren, T.; Ding, G.; Chen, J.; Pu, H. A dynamic model for FLNG spiral wound heat exchanger with multiple phase-change streams based on moving boundary method. *J. Nat. Gas Sci. Eng.* **2016**, *34*, 657−669.
(23) Cao, W. S.; Lu, X. S.; Gu, A. Z.; et al. Simulation of small-scale natural gas liquefaction flows in skid-mounted package[J]. *J. Chem. Ind. Eng.* **2006**, *57*, 1290−1295.
(24) Cao, W. S.; Lu, X. S.; Lin, W. S.; et al. Natural gas purification and liquefaction process of smal-l scale LNG project in skid-mounted package[J]. *J. Chem. Ind. Eng.* **2009**, *60*, 100−105.
(25) Dong, L. F.; Wu, X.; Liu, K.; Sun, Q. C. Influence of Sloshing Conditions on the Pressure Drop and Heat Transfer of a Single-Layer Spiral-Wound LNG Heat Exchanger. *ACS Omega* **2023**, *8*, 11310−11317.
(26) Mu, L.; Rutkowski, S.; Si, T.; Gai, M.; Wang, J.; Tverdokhlebov, S. I.; Frueh, J. A reduction of settlement probability of Chlorella vulgaris on photo-chemically active ceramics with hierarchical nano-structures. *Colloids Surf. A Physicochem. Eng. Asp.* **2021**, *610*, 125898.
(27) Mu, L.; Rutkowski, S.; Gai, M.; Tverdokhlebov, S. I.; Frueh, J. Copper alginate surface for perpetual Self-Polishing and Anti-Biofouling compound release. *Appl. Surf. Sci.* **2021**, *569*, 151087.

https://doi.org/10.1021/acsomega.3c02983
ACS Omega 2023, 8, 27467−27481